HHS Public Access

Author manuscript

Biomaterials. Author manuscript; available in PMC 2017 July 17.

Published in final edited form as:

Biomaterials. 2016 September ; 102: 239–248. doi:10.1016/j.biomaterials.2016.06.030.

A novel cationic lipid with intrinsic antitumor activity to facilitate gene therapy of TRAIL DNA

Cong Luo[a,b,1], **Lei Miao**[a,1], **Yi Zhao**[a], **Sara Musetti**[a], **Yuhua Wang**[a], **Kai Shi**[a,b], and **Leaf Huang**[a,*]

[a]Division of Molecular Pharmaceutics and Center for Nanotechnology in Drug Delivery, Eshelman School of Pharmacy, University of North Carolina at Chapel Hill, Chapel Hill, NC, 27599, USA

[b]Department of Pharmaceutics, School of Pharmacy, Shenyang Pharmaceutical University, Shenyang, 110016, PR China

Abstract

Metformin (dimethylbiguanide) has been found to be effective for the treatment of a wide range of cancer. Herein, a novel lipid (1,2-di-(9*Z*-octadecenoyl)-3-biguanide-propane (DOBP)) was elaborately designed by utilizing biguanide as the cationic head group. This novel cationic lipid was intended to act as a gene carrier with intrinsic antitumor activity. When compared with 1,2-di-(9*Z*-octadecenoyl)-3-trimethylammonium-propane (DOTAP), a commercially available cationic lipid with a similar structure, the blank liposomes consisting of DOBP showed much more potent antitumor effects than DOTAP in human lung tumor xenografts, following an antitumor mechanism similar to metformin. Given its cationic head group, biguanide, DOBP could encapsulate TNF-related apoptosis-inducing ligand (TRAIL) plasmids into Lipid-Protamine-DNA (LPD) nanoparticles (NPs) for systemic gene delivery. DOBP-LPD-TRAIL NPs demonstrated distinct superiority in delaying tumor progression over DOTAP-LPD-TRAIL NPs, due to the intrinsic antitumor activity combined with TRAIL-induced apoptosis in the tumor. These results indicate that DOBP could be used as a versatile and promising cationic lipid for improving the therapeutic index of gene therapy in cancer treatment.

Keywords

Cationic lipid; Metformin; Biguanide; Intrinsic antitumor activity; TRAIL; Nanoparticles

1. Introduction

Gene therapy is an efficient therapeutic strategy for cancer treatment [1]. However, intravenous delivery of nucleic acid based bioactive agents is still a major challenge. Viral gene carriers have long been criticized for their potential risk of immunogenicity and toxicity [2]. Non-viral systems may offer safer profiles and hold great potential for systemic gene delivery, but favorable clinical outcomes are still a long way off, primarily due to ineffective delivery mechanisms [2,3].

*Corresponding author. leafh@email.unc.edu (L. Huang).

[1]The authors contributed equally to this work.

The TNF-related apoptosis-inducing ligand (TRAIL) is a good candidate for cancer therapy due to its specific antitumor activity, which reduces risk to normal cells [4]. TRAIL has exhibited potent antitumor activity against a variety of tumors by inducing apoptosis in tumor cells, including human non-small-cell lung cancer (NSCLC) [4,5]. In addition to its strong antitumor activity, TRAIL presents no systemic toxicity in animals [6]. TRAIL-induced apoptosis is mediated by the death receptor pathway in tumor cells [7]. The binding of TRAIL to death domain-containing receptors on the cell surface will lead to the caspase-dependent irreversible apoptosis [7]. However, the application of TRAIL in cancer therapy is greatly limited by its short half-life *in vivo* [8]. Additionally, although TRAIL-targeted therapy holds great potential for cancer treatment, the clinical results of TRAIL have shown limitations, including inefficient delivery to tumor site, the complexity of the pathways, and resistance mechanisms [9]. Therefore, it is necessary to develop suitable nano-sized vehicles for TRAIL systemic delivery.

Metformin (dimethylbiguanide) is commonly used for patients with type II diabetes mellitus [10]. This cationic drug has well-established efficacy and a good safety profile, even at doses as high as 2 g/day, due to its very low toxicity [10]. More interestingly, metformin demonstrated significant antitumor activity against a wide range of cancers, including human NSCLC [10]. In our previous study, a cationic polymer of metformin (PolyMet) with intrinsic antitumor activity and low toxicity was designed and applied in siRNA delivery [11]. The biguanide groups of PolyMet can be used simultaneously as the cationic blocks for gene condensation and the chemotherapeutic agent for cancer treatment [11].

Designing carrier materials with intrinsic antitumor activity is an ideal strategy for cancer therapy. Therefore, we further hypothesized that biguanide could also be utilized as the cationic head group for a new cationic lipid, similar to 1,2-di-(9*Z*-octadecenoyl)-3-trimethylammonium-propane (DOTAP, a commercially available cationic lipid). Based on this rationale, we designed a DOTAP-like cationic lipid by changing the trimethylammonium of DOTAP to biguanide (Fig. 1A), namely 1,2-di-(9*Z*-octadecenoyl)-3-biguanide-propane (DOBP). DOBP was developed as a promising cationic lipid with intrinsic antitumor activity to facilitate gene therapy in cancer treatment. The biguanide group of DOBP acted similarly to metformin and perform antitumor activity by activating the AMPK signaling pathway [10]. And several studies have indicated that activation of AMPK signaling pathway could significantly sensitize TRAIL-induced apoptosis of human tumor cells [12–14]. Based on this rationale, we used a well-established Lipid-Protamine-DNA (LPD) formulation [15] to test the antitumor efficacy of the TRAIL plasmid DNA delivered by DOBP-LPD nanoparticles (NPs) (Fig. 1B) in a NSCLC model. The combined effect of DOBP and TRAIL was demonstrated.

2. Experimental section

2.1. Materials

Oleic acid, *N*-Boc-3-amino-glycerine, hydrochloride acid solution in 1,4-dioxane, dicyandiamide, protamine and cholesterol were purchased from Sigma-Aldrich. 1,2-dioleoyl-3-trimethylammonium-propane chloride salt (DOTAP) was obtained from Avanti Polar Lipids, Inc. (Alabaster, AL). 1,2-distearoryl-*sn*-glycero-3-phosphoethanolamine-*N*-

[methoxy(polyethyleneglycol-2000)] ammonium salt (DSPE-PEG2000) was purchased from NOF America Corporation. DSPE-PEG-Anisamide (DSPE-PEG-AA) was synthesized based on the previous established protocols [16], and DSPE-PEG-AA was used to specifically target to H460 cells that overexpress sigma receptors for enhanced cellular uptake of liposomes and LPD NPs [17]. An expression vector containing the human TRAIL open reading frame was purchased from InvivoGen (San Diego, CA). Primers for PCR and qPCR were purchased from Integrated DNA.

2.2. Synthesis of DOBP

2.2.1. Synthesis of 1,2-di-(9Z-octadecenoyl)-3-amino-propane (DOAP)—Oleic acid (3 mmol) was dissolved in 20 mL of dichloromethane, then *N*-Boc-3-amino-glycerine (1 mmol), EDC (3 mmol) and DMAP (3 mmol) were added. The reaction mixture was stirred at 25 °C for 24 h under nitrogen. Post-reaction, *N*-Boc-DOAP was obtained and purified by silica column chromatography (petroleum ether/ethyl acetate = 20:1). The Boc protection of the product was deprotected using hydrochloride acid solution in 1,4-dioxane, and DOAP (chloride salt) was obtained with a yield of 85%. The chemical structure of DOAP (chloride salt) was confirmed by nuclear magnetic resonance spectroscopy (NMR, 400 MHz ^{1}H NMR, BRUKER AV-400).

2.2.2. Synthesis of 1,2-di-(9Z-octadecenoyl)-3-biguanide-propane (DOBP)—DOAP (chloride salt, 1 mmol) was dissolved in 20 mL of 1,4-dioxane, and dicyandiamide (2 mmol) in 2 mL of DMF was added. $FeCl_3$ (1 mmol) was utilized as catalyst. The reaction mixture was stirred at 70°C for 48 h under nitrogen. The reaction mixture was washed with 5% hydrochloride acid to remove the $FeCl_3$ and free dicyandiamide, and dried with anhydrous sodium sulfate. Sodium sulfate was filtered, and the solvent was evaporated under vacuum. DOBP (chloride salt) was purified by silica column chromatography (dichloromethane/methanol = 30:1) with a yield of 30%. The chemical structure of DOBP (chloride salt) was confirmed by nuclear magnetic resonance spectroscopy (NMR, 400 MHz ^{1}H NMR, BRUKER AV-400).

2.3. Preparation of liposome and LPD NPs

DOBP or DOTAP and cholesterol (1:1, mol/mol) were dissolved in chloroform and the solvent was evaporated under reduced pressure. The lipid film was hydrated overnight with distilled water to make the final concentration 10 mM DOBP or DOTAP and 10 mM cholesterol. The DOBP-liposome (Lipo-DOBP) and the DOTAP-liposome (Lipo-DOTAP) were sequentially extruded through 400 nm, 200 nm, 100 nm and 50 nm polycarbonate membranes (Millipore, Billerica, MA), respectively. The polyplex core of the LPD NPs was prepared by mixing 26 μg protamine in100 μL 5% glucose with equal volume of 50 μg plasmid in 5% glucose. The mixture was incubated at room temperature for 10 min before 60 μL of Lipo-DOBP or Lipo-DOTAP (10 mmol/L each) were added. PEGylation and targeting modification were achieved by adding 15 mol% DSPE-PEG and DSPE-PEG-AA in the formulations with further performed at 60 °C for 15 min. The size and zeta potential were measured by using Zetasizer (Nano ZS, Malvern Co., UK). The morphology of the LPD NPs was observed by JEOL 100CX II transmission electron microscopy (TEM) (JEOL, Japan). NPs were negatively stained with 2% uranyl acetate. To investigate the

stability of LPD NPs under serum condition, LPD NPs were incubated in PBS (pH 7.4) supplemented with 5% of fetal bovine serum (FBS) for 12 h at 37 °C, and the mean diameter of the NPs was determined at timed intervals.

2.4. Cell culture

H460 human NSCLC cells and MRC-5 human fetal lung fibroblast cells were originally obtained from American Type Culture Collection (ATCC). The cells were cultured in RPMI 1640 medium supplemented with 10% (v/v) fetal bovine serum (FBS), penicillin (100 units/mL) and streptomycin (100 μg/mL) in a humidified atmosphere of 5% CO_2 at 37 °C.

2.5. In vitro cytotoxicity of blank liposome

The *in vitro* cytotoxicity of metformin, Lipo-DOTAP and Lipo-DOBP was investigated by 3-(4,5-dimethylthiazol-2-yl)-2,5-diphenyltetrazolium bromide (MTT) assay in H460 cells and MRC-5. Briefly, cells were incubated in 100 μL of complete culture medium in 96-well plates at a density of 5000 cells/well for 24 h. After pre-incubation, the cells were exposed to serial dilutions of metformin, Lipo-DOTAP and Lipo-DOBP at different concentrations for 4 h, and washed and further incubated for 48 h. The cells without any treatment were utilized as control.

2.6. In vitro apoptosis and necrosis assay

H460 cells were seeded into a 6-well plate (1.0×10^6 cells/well) for 24 h. After pre-incubation, the cells were exposed to Lipo-DOTAP (20 and 50 μM), Lipo-DOBP (20 and 50 μM) and PEI (1.25 and 12.5 μM) for 6 h. Then, the cells were washed with PBS and trypsinized. Apoptosis and necrosis analysis was evaluated according to the manufacturer's protocols (Beckon Dickinson, CA). Annexin V-FITC (FL1)/PI (FL2) fluorescence signals were analyzed by flow cytometry on a BD FACSAria instrument (Beckon Dickinson, CA).

2.7. Cellular uptake and intracellular trafficking of DOBP-LPD NPs

For the visualization of cellular uptake and intracellular trafficking of DOBP-LPD-NPs, a hydrophobic dye DiI (Sigma, MO) was encapsulated into the lipid layer of the NPs. At the same time, Cy5 labelled DNA was prepared using Label IT® (Mirus, Madison, WI, USA) and encapsulated into the polyplex core of the NPs. The double labelled NPs (with or without AA) was then incubated with NCI-H460 cells, which were pre-seeded in LabTek Chambered Coverglass at a density of 5×10^4 cells/well. At 0.5, 2, and 6 h post incubation, cells were washed three times with cold DPBS and then subjected to endosome/lysosome and nucleus staining by incubation with Lysotracker Green (1 μg/mL) and Hoechst 33342 (5 μg/mL), respectively. After washing with DPBS, cover slips were mounted on slides and examined by confocal laser scanning microscopy (Zeiss LSM 510 Meta, Germany).

2.8. Animals

Female nude mice (4–6 weeks old) were used in the animal studies. Animals were purchased from National Cancer Institute (Bethesda, MD) and bred by the Division of Laboratory Animal Medicine (DLAM) at University of North Carolina at Chapel Hill. To establish the H460 NSCLC xenograft models, 5×10^6 cells in 100 μL of PBS were injected

subcutaneously into the right flank of the mice. All animal studies were carried out according to the protocols approved by the University of North Carolina at Chapel Hill's Institutional Animal Care and Use Committee.

2.9. In vivo antitumor activity of blank liposomes

Human H460 NSCLC cells (5×10^6 cells/100 μL) in PBS were inoculated subcutaneously into the female nude mice. When the tumor size was approximately 80 mm^3, H460 xenografts tumor-bearing nude mice were randomized to four groups (five mice per group): untreated control (PBS), metformin solution, Lipo-DOTAP and Lipo-DOBP. The mice received treatment through tail veins every other day for a total of 5 injections with an equivalent metformin dose of 5 mg/kg. Lipo-DOBP and Lipo-DOTAP were administrated at an equivalent molar dose of metformin (30 μmol/kg of DOBP or DOTAP). Tumor volume and body weight were measured every day. Mice were sacrificed one day after the last injection, and serum was collected for hepatic and renal function analysis.

2.10. Western-Blot analysis

Tumor samples were lysed by a Radio-Immunoprecipitation Assay (RIPA) buffer. A bicinchoninic acid (BCA) assay (Invitrogen, CA) was used to determine the protein concentration in the tumors according to the manufacturer's protocols. The protein solution was diluted by sample buffer (4×) containing reducing reagent and heated at 95 °C for 5 min. Protein was separated by 4%–12% SDS-PAGE electrophoresis (Invitrogen), and then transferred to polyvinylidene difluoride (PVDF) membranes (Bio-Rad). The membranes were blocked with 5% non-fat dry milk (Bio-Rad) at room temperature for 1 h and then incubated with primary antibodies overnight at 4 °C. The membranes were washed and further incubated with a secondary antibody (1:4000 dilution) at room temperature for 1 h, and then detected using the Pierce ECL Western Blotting Substrate (Thermo Fisher Scientific, IL). GAPDH was used as the control.

2.11. Pharmacokinetics and biodistribution of LPD NPs

A trace amount of ^3H labelled cholesteryl hexadecyl ether (PerkinElmer, MA) were mixed with other lipids while preparing the liposomes. Mice were injected IV via the tail vein with ^3H-labelled DOBP-LPD NPs or DOTAP-LPD NPs (with same ^3H levels, n = 3). At 5 min, 15 min, 30 min, 1, 2, 4, 8, 16, 24 h post-injection, blood samples were collected from the saphenous vein using a heparinized capillary tube. The mice were sacrificed after endpoint (24 h) and major organs were collected afterwards. Ten to 20 mg of blood, or ~100 mg tissues were immediately mixed with 10 × NCS® II Tissue Solubilizer (Amersham Biosciences, Inc) and digested at 60 °C overnight. Two hundred μL of hydrogen peroxide (30% in water, Fisher) was added to the samples and vortexed to bleach the color, and the sample was then mixed with 4 mL scintillation cocktail (Fisher Inc). The ^3H radioactivity in the blood and tissue samples were counted using a liquid scintillation analyzer (TRI-CARB 2900 TR, Packard Bioscience Co.).

2.12. In vivo antitumor activity of LPD NPs

Human H460 NSCLC xenograft was constructed by the same methods in female nude mice. GFP plasmids were used as the control of TRAIL plasmids. When the tumor size was approximately 150 mm^3, H460 xenografts tumor-bearing nude mice were randomized to five groups (five mice per group): untreated control (PBS), DOTAP-LPD-GFP NPs, DOBP-LPD-GFP NPs, DOTAP-LPD-TRAIL NPs and DOBP-LPD-TRAIL NPs. The mice received tail vein injections of treatments every other day for a total of 5 injections with a dose of 50 μg DNA/mouse (0.6 μmol of DOBP or DOTAP/mouse). Tumor volume and body weight were measured every day. Mice were sacrificed two days after the last injection, and serum was collected for hepatic and renal function analysis.

2.13. TUNEL assay and H&E staining

The tumor and major organs were collected and fixed with 4% paraformaldehyde in PBS overnight and processed with paraffin embedding by the UNC histology facility. Apoptosis of tumor cells was then explored by TdT-dependent dUTP-biotin nick end labeling (TUNEL) assay using an apoptosis detection kit (Promega, Madison, WI) according to the manufacturer's instructions. All samples were observed with an Eclipse Ti-U inverted microscope (Nikon Corp., Tokyo, Japan) and quantified using Image J software based on the manufacturer's instructions. The formalin-embedded tissues were stained by hematoxylin and eosin (H&E) to identify the pathological change of major organs.

2.14. Quantitative Real-time PCR (qPCR) assay

The total RNA of tumor tissues was extracted using RNeasy Kit (Qiagen, CA). The cDNA was reverse-transcribed with the First-Strand Synthesis System for qPCR (Invitrogen, NY). Then cDNA (~100 ng) was amplified using the Taqman® Universal Probes Supermix system (Biorad, CA) with Taqman® primer against human TRAIL (Hs00234355_ml, Invitrogen CA). Reactions were conducted with the 7500 Real-Time PCR System, and the 7500 software was used to analyze the data. GAPDH (Taqman® primer against human GAPDH, hs02758991_g1) was utilized as the endogenous control.

2.15. In vitro and in vivo transfection of TRAIL DNA

To investigate the *in vitro* transfection of TRAIL DNA, H460 cells were grown until 80% confluent in six-well plates. Then DOBP-LPD-TRAIL NPs, DOTAP-LPD-TRAIL NPs and DOBP-LPD-GFP NPs were added to each well in the presence of OptiMEM medium with final concentration of 1 μg plasmid/mL. Medium was refreshed 4 h after transfection. The remaining cells were treated for another 48 h. The transfection efficiency of TRAIL was determined by Western-Blot analysis using primary antibody against human TRAIL (Prosci) and with GAPDH as a loading control. For *in vivo* transfection, the expression levels of TRAIL DNA in tumor tissues were determined by qPCR and Western-Blot assay, respectively.

2.16. Statistical analysis

Student's *t*-test and one-way analysis of variance (ANOVA) were utilized to analyze the differences of the groups, and $P < 0.05$ was considered statistically significant. Data were shown as mean ± SD.

3. Results and discussions

3.1. Rational design of 1,2-di-(9Z-octadecenoyl)-3-biguanide-propane (DOBP)

To test our hypothesis, a novel cationic lipid (DOBP) was designed and synthesized by using biguanide as the cationic head (Fig. 2). Oleic acid was coupled to the hydroxyl position of *N*-Boc-3-amino-glycerine, the Boc protection was then removed to obtain 1,2-di-(9*Z*-octadecenoyl)-3-amino-propane (DOAP). Finally, Dicyandiamide was conjugated to the amino group of DOAP to obtain DOBP. DOBP was intended as a versatile lipid that could be applied as a gene carrier as well as an anticancer drug. As shown in Fig. S1, the NMR spectrum confirmed the successful synthesis of DOBP. With the disappearing of the peak of ammonium salt, the typical peaks of biguanide can be found around the δ value of 7 ppm.

3.2. Preparation of blank liposomes and LPD NPs

Both the blank liposomes (Lipo-DOBP and Lipo-DOTAP) and the LPD nano-formulations (DOBP-LPD-GFP NPs, DOBP-LPD-TRAIL NPs, DOTAP-LPD-GFP NPs and DOTAP-LPD-TRAIL NPs) were prepared following a well-established protocol developed by our lab [15]. Dynamic light scattering (DLS) was utilized to determine their particle size and zeta potential. As shown in Table S1, the average diameter of Lipo-DOBP and Lipo-DOTAP was 120–130 nm, and the zeta potential was determined to be ~50 mV. The particle size of LPD formulations was determined to be 140–150 nm with a slightly decreased positive zeta potential (~37 mV) due to the encapsulation of the negative charged polyplex core (−28.4 mV). TEM images analyzing particle morphology confirmed the successful fabrication of LPD NPs (Fig. S2). Moreover, we further investigated the stability of the prepared LPD NPs in PBS (pH 7.4) supplemented with 5% of fetal bovine serum (FBS) for 12 h at 37 °C. As shown in Fig. S3, the prepared LPD NPs showed good stability with no significant variation of their mean diameter over a period of 12 h. Successfully formulating TRAIL plasmids into DOBP-LPD-TRAIL NPs suggested that this novel cationic lipid could be used for systemic gene delivery, due to its biguanide head group and structural similarity to DOTAP.

3.3. In vitro cytotoxicity of blank liposomes

To test the anticancer potency of DOBP, the *in vitro* cytotoxicity of metformin, Lipo-DOBP and Lipo-DOTAP was evaluated in H460 cells. As shown in Fig. 3, metformin showed almost no cytotoxicity at the dose tested, but significant cytotoxicity of metformin could be observed at a higher dose (data not shown). Interestingly, Lipo-DOBP showed the highest cytotoxicity when compared with both metformin and Lipo-DOTAP. Notably, Lipo-DOTAP also showed some cytotoxicity at high dose (2 mM) due to its non-specific antitumor activity [18]. Metformin is different from the conventional cytotoxic agents (e.g. paclitaxel and doxorubicin), the lower *in vitro* cytotoxicity of metformin corresponds to its good safety profile, as this drug is used in the clinics at very high doses due to very low toxicity [10]. By

contrast, “formulating” the biguanide (DOBP) into the nano-sized liposomes greatly enhanced its cytotoxicity to tumor cells. Additionally, the *in vitro* cytotoxicity of Lipo-DOBP and Lipo-DOTAP were evaluated in human fetal lung fibroblast cells (MRC-5 cells). As shown in Fig. S4, within the same concentration range of the cytotoxicity test in H460 cells, Lipo-DOBP and Lipo-DOTAP showed much less cytotoxicity in MRC-5 cells than in H460 cells, probably due to the fast proliferation of the latter.

3.4. Cellular uptake and intracellular trafficking of DOBP-LPD NPs

The cellular uptake and dynamic intracellular trafficking of DOBP-LPD NPs were investigated using confocal microscopy. The function of anisamide (AA) as targeting ligand were also evaluated. Cy5-labelled DNA (Cy5-DNA, shown as magenta) and hydrophobic dye DiI incorporated into Lipo-DOBP (shown as red) were utilized to track the intracellular distribution of DNA and carrier, respectively. H460 cells were incubated with the double-labelled DOBP-LPD NPs (with or without AA) for different time periods as specified in Fig. 4. The cell samples were co-stained for multiple organelles, including cell nuclei (with Hoechst, blue) and lysosomes (with LysoTracker Green, green). Tracking the double-labelled NPs relative to these cell organelles provided information how the plasmid delivered by DOBP-LPD NPs were transported through the cytoplasm into the nucleus. As shown in Fig. 4B and D, the overall internalization of lipid vector and plasmid were increased gradually with time. As expected, AA could significantly facilitate the cellular uptake of LPD NPs, which provides the basic rationale for choosing AA as a targeting ligand for *in vivo* therapeutic application. The overall fluorescence (both Cy5-DNA and DiI) of cells incubated with non-targeted NPs were relatively weak over the course of the time monitored. The accumulation of NPs into lysosomes were observed only at 6 h after incubation. The binding and internalization process occurred rapidly in the AA-DOBP-LPD NPs incubated cells. As shown in Panel C and E, both DiI and Cy5-DNA carried by AA-DOBP-LPD NPs were accumulated into the lysosome (co-localized with LysoTracker, shown as yellow and white, respectively) rapidly within 0.5 h of incubation. The co-localization of Cy5-DNA and DiI suggested that the NPs remained intact at this time point. The endosomal release of AA-DOBP-LPD NPs was observed at 2 h after incubation, as large amount of DiI was scattered throughout the cytoplasm. As expected, dissociation of plasmid from the lipid vector occurred upon endosomal release (Panel F, 2 h). As the time increased, the dissociated plasmids were gradually translocated into the nucleus (panel D–F, 6 h), most likely due to the nucleus targeting function of protamine [19]. Overall, the intracellular trafficking study suggested that the novel cationic lipid DOBP and the targeting ligand AA, could efficiently enable the internalization, endosomal escape of the LPD NPs, allowing plasmid to dissociate from the lipid and effectively transport into the nucleus for transcription and gene expression.

3.5. In vivo antitumor activity of blank liposomes

The *in vivo* antitumor efficacy of metformin, Lipo-DOBP, and Lipo-DOTAP was initially evaluated in nude mice bearing H460 xenograft tumors. Metformin and Lipo-DOBP were administrated intravenously every other day for a total of 5 injections at a dose equivalent to 5 mg/kg of metformin, and Lipo-DOTAP was administrated at an equivalent molar dose of Lipo-DOBP. Mice that were dosed only with PBS were used as a control. As shown in Fig.

5, both Lipo-DOBP and metformin showed significant antitumor efficacy, with a distinctly delayed tumor progression. Lipo-DOTAP were also able to somewhat suppress tumor growth, due to the non-specific antitumor activity of DOTAP which has been reported before [18]. Notably, despite the low cytotoxicity of metformin *in vitro*, it demonstrated significant antitumor activity *in vivo*. Indeed, distinguished from the conventional cytotoxic agents, metformin delays the tumor growth and proliferation via acting on cell signaling pathways [10].

A TUNEL assay (Fig. 5D and E) demonstrated significant tumor cell apoptosis in mice treated with metformin, Lipo-DOBP and Lipo-DOTAP. Both metformin and Lipo-DOBP induced higher rates of apoptosis in tumors over Lipo-DOTAP. Importantly, no significant change in body weight was observed across all mouse populations (Fig. 6A). The hematological parameters, aspartate aminotransferase (AST), alanine aminotransferase (ALT) levels, blood urea nitrogen (BUN) and creatinine, showed no indication of toxicity (Fig. 6B). Moreover, the *in vitro* apoptosis and necrosis studies indicated that both Lipo-DOBP and Lipo-DOTAP showed much less late apoptosis and necrosis when compared with a frequently-used cationic polymer PEI (Fig. S5). And no noticeable histological changes were observed in H&E-stained tissue sections of major organs (Fig. S7). These results suggest that DOBP with intrinsic antitumor activity elicited no significant off-target toxicities to major organs and tissues.

3.6. Antitumor mechanism of DOBP

As described before, Lipo-DOBP exhibited comparable *in vivo* antitumor efficacy with metformin. We then investigated the antitumor mechanism of DOBP. Since the C–N bond between the biguanide moiety is highly stable and the biguanide group is the key point for the antitumor activity of metformin [10], we inferred that the biguanide moiety on DOBP directly induced anti-tumor efficacy without being cleaved off. Several studies have indicated that metformin inhibits cancer cells growth by activating the AMP-activated protein kinase (AMPK) and inhibiting the mammalian target of rapamycin (mTOR) pathways [20,21]. AMPK is a metabolic tumor suppressor that affects glucose and lipid metabolism, and mTOR is a downstream effector of AMPK. The degree of phosphorylation of AMPK and mTOR plays a crucial role in the proliferation and survival of cancer cells [22,23]. Moreover, a recent study published by our group demonstrated that a non-cleavable biguanide group (PolyMet) could directly induce tumor apoptosis through activation of the AMPK and inhibiting the mTOR pathways [11]. Therefore, to address the intrinsic antitumor activities of the biguanide containing-DOBP, the regulation of these two pathways were evaluated by Western-Blot assay. As shown in Fig. 5C, AMPK-α was phosphorylated at a much higher rate in tumor tissues that was treated with metformin and Lipo-DOBP than with PBS and Lipo-DOTAP. In contrast, mTOR phosphorylation was down-regulated in metformin and Lipo-DOBP treated tissues. The Western blot results indicated that DOBP followed a similar antitumor mechanism as metformin, and further confirmed our hypothesis that the biguanide head of DOBP made it a versatile cationic lipid with intrinsic antitumor activity.

3.7. Pharmacokinetics and biodistribution of LPD NPs

Pharmacokinetics and biodistribution studies of DOBP-LPD NPs and DOTAP-LPD NPs were evaluated in nude mice with ^{3}H-cholesterol as a label. As shown in Fig. S6, DOBP-LPD NPs and DOTAP-LPD NPs demonstrated similar pharmacokinetic behaviors and biodistribution in major organs. These results could be attributed to the similar chemical structure of DOBP with DOTAP and the same LPD nano-formulation. Additionally, most NPs were accumulated in liver and spleen due to the abundant blood and the presence of reticuloendothelial system (RES).

3.8. In vivo antitumor activity of LPD NPs

Lipo-DOBP showed significant antitumor activity *in vitro* and *in vivo*. We then investigated the anticancer efficacy of TRAIL-encapsulating LPD NPs modified with DSPE-PEG-AA. In this study, GFP plasmids were used as the control DNA. The *in vivo* antitumor efficacy of LPD formulations (DOBP-LPD-GFP NPs, DOTAP-LPD-GFP NPs, DOBP-LPD-TRAIL NPs and DOTAP-LPD-TRAIL NPs) was evaluated in nude mice bearing H460 xenograft tumors, with PBS injections as a control. This study was performed on relatively large tumors (over 150 mm^{3}). Treatment was administered via tail vein injections every other day for a total of 5 injections with a dose of 50 μg DNA/mouse. As shown in Fig. 7, DOBP-LPD-GFP NPs, DOTAP-LPD-TRAIL NPs and DOBP-LPD-TRAIL NPs all demonstrated distinct antitumor activity, but DOBP-LPD-TRAIL NPs exhibited significant superiority over both DOBP-LPD-GFP NPs and DOTAP-LPD-TRAIL NPs. This is likely due to the intrinsic anticancer activity of DOBP combined with TRAIL-induced apoptosis. Activation of AMPK signaling pathway could significantly sensitize TRAIL-induced apoptosis of human tumor cells [12–14]. As shown earlier (Fig. 5C), AMPK activation was observed in Lipo-DOBP treated groups. In addition, DOTAP-LPD-GFP NPs were unable to significantly suppress tumor growth when compared with PBS group. These results indicated that DOBP, a versatile cationic lipid, could be used as a new cationic lipid with intrinsic antitumor activity to facilitate the gene therapy of TRAIL DNA.

A TUNEL assay was used to quantify apoptosis in tumor tissues after treatment. As shown in Fig. 7D and E, DOBP-LPD-GFP NPs, DOTAP-LPD-TRAIL NPs and DOBP-LPD-TRAIL NPs demonstrated significant tumor cell apoptosis in mice after treatment, and DOBP-LPD-TRAIL NPs showed distinct superiority over DOBP-LPD-GFP NPs and DOTAP-LPD-TRAIL NPs. In addition, no significant change in body weight was observed in any of the mice used in this study (Fig. 7C). The hematological parameters indicated no detectable damage (Fig. S8) and no noticeable histological changes were observed in H&E-stained tissue sections of major organs (Fig. S9). These results indicated that DOBP-LPD-TRAIL NPs, with combined antitumor activity of DOBP and TRAIL DNA, showed no significantly nonspecific toxicity to major organs and tissues.

3.9. In vitro and in vivo transfection of TRAIL DNA

To investigate the *in vitro* and *in vivo* transfection of TRAIL DNA, qPCR and Western-Blot assay were used to measure the gene expression in tumor tissues. As shown in Fig. 8, DOBP-LPD-TRAIL NPs and DOTAP-LPD-TRAIL NPs showed comparable TRAIL mRNA expression level. Consistently, these two formulations induced similar TRAIL protein

expression both *in vitro* and *in vivo* (Fig. S10). The enhanced TRAIL expression was seen over the background levels of endogenous TRAIL in the control groups. These results suggested that DOBP, with a very similar structure to DOTAP, transfected cells as efficiently as commercially available DOTAP. While DOBP-LPD-TRAIL NPs exhibited higher antitumor efficacy than that of DOTAP-LPD-TRAIL NPs, due to the intrinsic antitumor activity of gene carrier and the TRAIL-induced apoptosis in tumor cells. These results further confirmed our hypothesis that DOBP could be used as a versatile cationic carrier to facilitate gene therapy of TRAIL DNA.

4. Conclusions

Inspired by the antitumor activity of metformin, a novel cationic lipid (DOBP) with intrinsic antitumor activity was designed for systemic gene delivery in cancer therapy. For this new lipid, biguanide simultaneously acts as the cationic lipid for gene encapsulation and delivery, as well as the pharmacologically active treatment for cancer. DOBP showed comparable capacity of gene transfection with DOTAP, and exhibited potent antitumor activity *in vitro* and *in vivo* with a similar anticancer mechanism to metformin. As a result, DOBP-LPD-TRAIL NPs demonstrated distinct superiority in antitumor efficacy over DOTAP-LPD-TRAIL NPs due to the intrinsic antitumor activity of biguanide and the TRAIL-induced apoptosis in tumor cells. Therefore, DOBP, a novel versatile cationic lipid, provides a promising platform for systemic delivery of gene.

Supplementary Material

Refer to Web version on PubMed Central for supplementary material.

Acknowledgments

The work was financially supported by NIH grants CA149363, 100000002, and CA149387, and by the North Carolina Biotech Center Institutional Support Grant 2005-IDG-1016. We thank UNC Animal Histopathology Core and UNC Translational Pathology Laboratory for tissue processing. We also thank UNC-CH Genome Core for gene sequencing of TRAIL.

Appendix A. Supplementary data

Supplementary data related to this article can be found at http://dx.doi.org/10.1016/j.biomaterials.2016.06.030.

References

1. Huang L, Liu Y. In vivo delivery of RNAi with lipid-based nanoparticles. Annu Rev Biomed Eng. 2011; 13:507–530. [PubMed: 21639780]
2. Mokhtarzadeh A, Alibakhshi A, Yaghoobi H, Hashemi M, Hejazi M, Ramezani M. Recent advances on biocompatible and biodegradable nanoparticles as gene carriers. Expert Opin Biol Ther. 2016:1–15.
3. Luo C, Sun J, Sun B, He Z. Prodrug-based nanoparticulate drug delivery strategies for cancer therapy. Trends Pharmacol Sci. 2014; 35:556–566. [PubMed: 25441774]
4. Voortman J, Resende TP, Abou El Hassan MA, Giaccone G, Kruyt FA. TRAIL therapy in non-small cell lung cancer cells: sensitization to death receptor-mediated apoptosis by proteasome inhibitor bortezomib. Mol Cancer Ther. 2007; 6:2103–2112. [PubMed: 17620439]

5. Abou El Hassan MA, Mastenbroek DC, Gerritsen WR, Giaccone G, Kruyt FA. Overexpression of Bcl2 abrogates chemo- and radiotherapy-induced sensitisation of NCI-H460 non-small-cell lung cancer cells to adenovirus-mediated expression of full-length TRAIL. Br J Cancer. 2004; 91:171–177. [PubMed: 15173860]
6. Kagawa S, He C, Gu J, Koch P, Rha SJ, Roth JA, et al. Antitumor activity and bystander effects of the tumor necrosis factor-related apoptosis-inducing ligand (TRAIL) gene. Cancer Res. 2001; 61:3330–3338. [PubMed: 11309289]
7. Yoo J, Choi S, Hwang KS, Cho WK, Jung CR, Kwon ST, et al. Adeno-associated virus-mediated gene transfer of a secreted form of TRAIL inhibits tumor growth and occurrence in an experimental tumor model. J Gene Med. 2006; 8:163–174. [PubMed: 16144019]
8. Kelley SK, Harris LA, Xie D, Deforge L, Totpal K, Bussiere J, et al. Preclinical studies to predict the disposition of Apo2L/tumor necrosis factor-related apoptosis-inducing ligand in humans: characterization of in vivo efficacy, pharmacokinetics, and safety. J Pharmacol Exp Ther. 2001; 299:31–38. [PubMed: 11561060]
9. Lim B, Allen JE, Prabhu VV, Talekar MK, Finnberg NK, El-Deiry WS. Targeting TRAIL in the treatment of cancer: new developments. Expert Opin Ther Targets. 2015; 19:1171–1185. [PubMed: 26004811]
10. Morales DR, Morris AD. Metformin in cancer treatment and prevention. Annu Rev Med. 2015; 66:17–29. [PubMed: 25386929]
11. Zhao Y, Wang W, Guo S, Wang Y, Miao L, Xiong Y, et al. PolyMetformin combines carrier and anti-cancer activities for in vivo siRNA delivery. Nat Commun. 2016; 7
12. Su RY, Chao Y, Chen TY, Huang DY, Lin WW. 5-Aminoimidazole-4-car-boxamide riboside sensitizes TRAIL- and TNF{alpha}-induced cytotoxicity in colon cancer cells through AMP-activated protein kinase signaling. Mol Cancer Ther. 2007; 6:1562–1571. [PubMed: 17513605]
13. Garcia-Garcia C, Fumarola C, Navaratnam N, Carling D, Lopez-Rivas A. AMPK-independent down-regulation of cFLIP and sensitization to TRAIL-induced apoptosis by AMPK activators. Biochem Pharmacol. 2010; 79:853–863. [PubMed: 19896469]
14. Nieminen AI, Eskelinen VM, Haikala HM, Tervonen TA, Yan Y, Partanen JI, et al. Myc-induced AMPK-phospho p53 pathway activates Bak to sensitize mitochondrial apoptosis. Proc Natl Acad Sci U S A. 2013; 110:E1839–E1848. [PubMed: 23589839]
15. Wang Y, Xu Z, Guo S, Zhang L, Sharma A, Robertson GP, et al. Intravenous delivery of siRNA targeting CD47 effectively inhibits melanoma tumor growth and lung metastasis. Mol Ther. 2013; 21:1919–1929. [PubMed: 23774794]
16. Banerjee R, Tyagi P, Li S, Huang L. Anisamide-targeted stealth liposomes: a potent carrier for targeting doxorubicin to human prostate cancer cells. Int J Cancer. 2004; 112:693–700. [PubMed: 15382053]
17. Li S, Chen Y, Hackett M, Huang L. Tumor-targeted delivery of siRNA by self-assembled nanoparticles. Mol Ther. 2008; 16:163–169. [PubMed: 17923843]
18. Yan W, Chen W, Huang L. Mechanism of adjuvant activity of cationic liposome: phosphorylation of a MAP kinase, ERK and induction of chemokines. Mol Immunol. 2007; 44:3672–3681. [PubMed: 17521728]
19. Pouton CW, Wagstaff KM, Roth DM, Moseley GW, Jans DA. Targeted delivery to the nucleus. Adv Drug Deliv Rev. 2007; 59:698–717. [PubMed: 17681634]
20. Dowling RJ, Zakikhani M, Fantus IG, Pollak M, Sonenberg N. Metformin inhibits mammalian target of rapamycin-dependent translation initiation in breast cancer cells. Cancer Res. 2007; 67:10804–10812. [PubMed: 18006825]
21. Yue W, Yang CS, DiPaola RS, Tan XL. Repurposing of metformin and aspirin by targeting AMPK-mTOR and inflammation for pancreatic cancer prevention and treatment. Cancer Prev Res Phila. 2014; 7:388–397. [PubMed: 24520038]
22. Zulato E, Bergamo F, De Paoli A, Griguolo G, Esposito G, De Salvo GL, et al. Prognostic significance of AMPK activation in advanced stage colorectal cancer treated with chemotherapy plus bevacizumab. Br J Cancer. 2014; 111:25–32. [PubMed: 24892446]

23. Kimura N, Tokunaga C, Dalal S, Richardson C, Yoshino K, Hara K, et al. A possible linkage between AMP-activated protein kinase (AMPK) and mammalian target of rapamycin (mTOR) signalling pathway. Genes Cells. 2003; 8:65–79. [PubMed: 12558800]

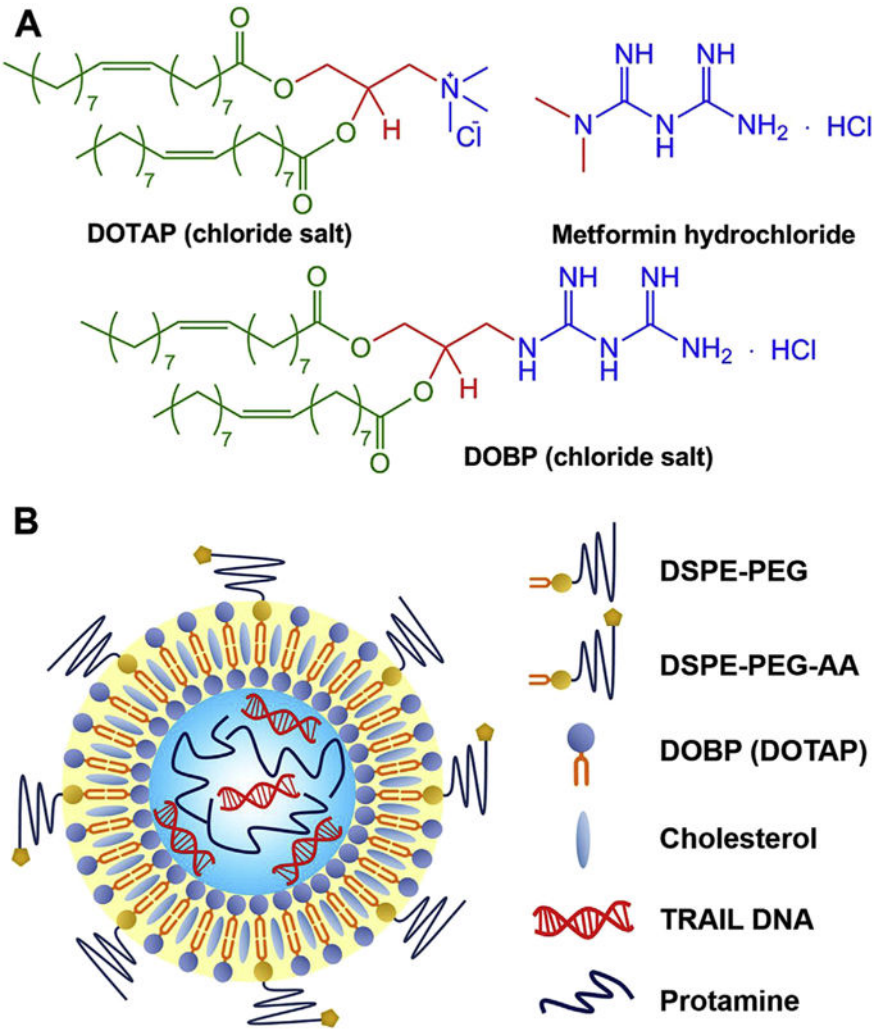

Fig. 1.

(A) Chemical structures of DOTAP, metformin and DOBP. (B) Schematic illustration of LPD-TRAIL NPs.

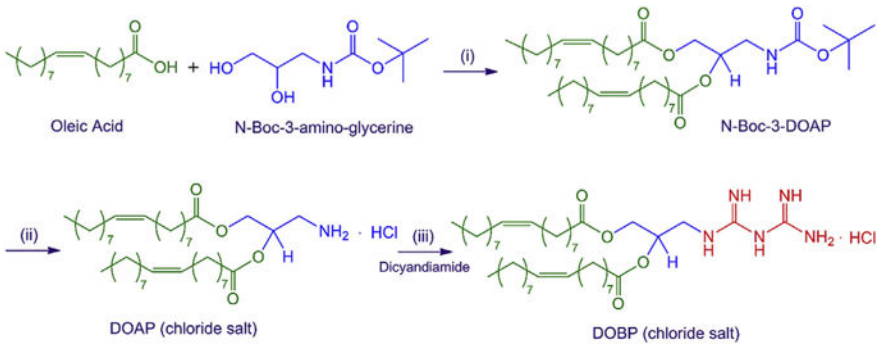

Fig. 2.

Synthesis routes of DOBP. (i) DCC, DMAP, r.t.; (ii) Hydrochloride acid solution in 1,4-dioxane; and (iii) $FeCl_3$.

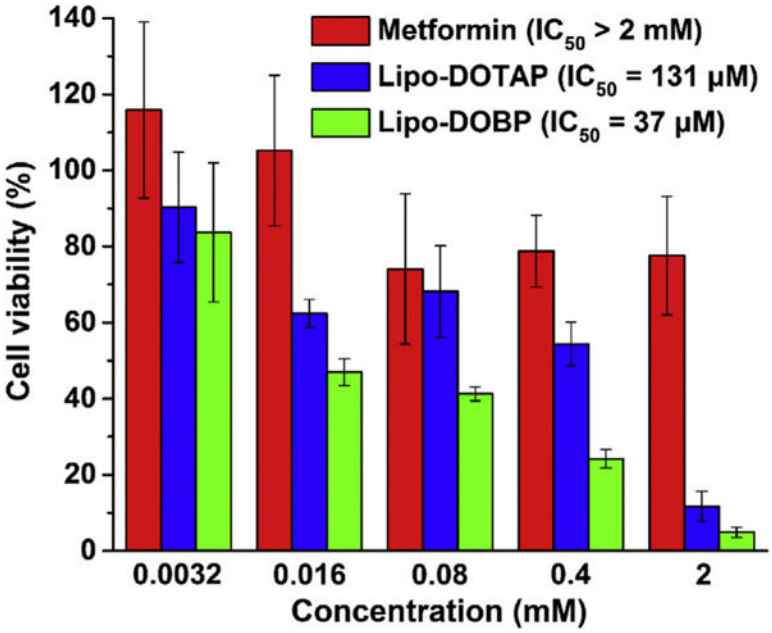

Fig. 3.

Representative dose-response curves of the MTT assays against H460 cells.

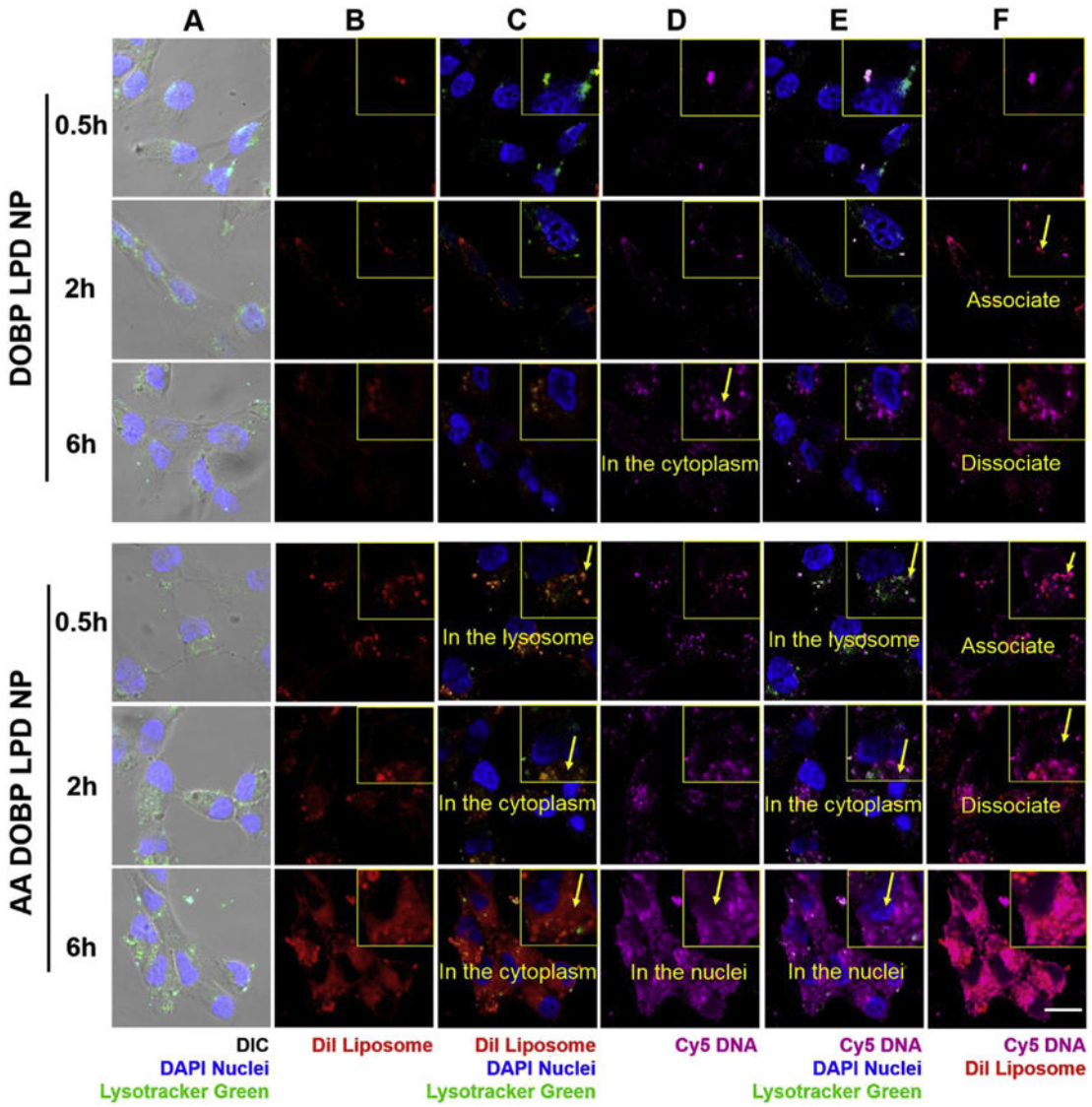

Fig. 4.

In vitro cellular uptake and intracellular trafficking of AA-DOBP-LPD NPs and AA-free DOBP-LPD NPs. (A) DIC/DAPI/Lysotracker Green. (B) DiI. (C) DiI/DAPI/Lysotracker Green. (D) Cy5 DNA. (E) Cy5 DNA/DAPI/Lysotracker Green. (F) Cy5 DNA/DiI. Scale bar represents 10 μm. (For interpretation of the references to color in this figure legend, the reader is referred to the web version of this article.)

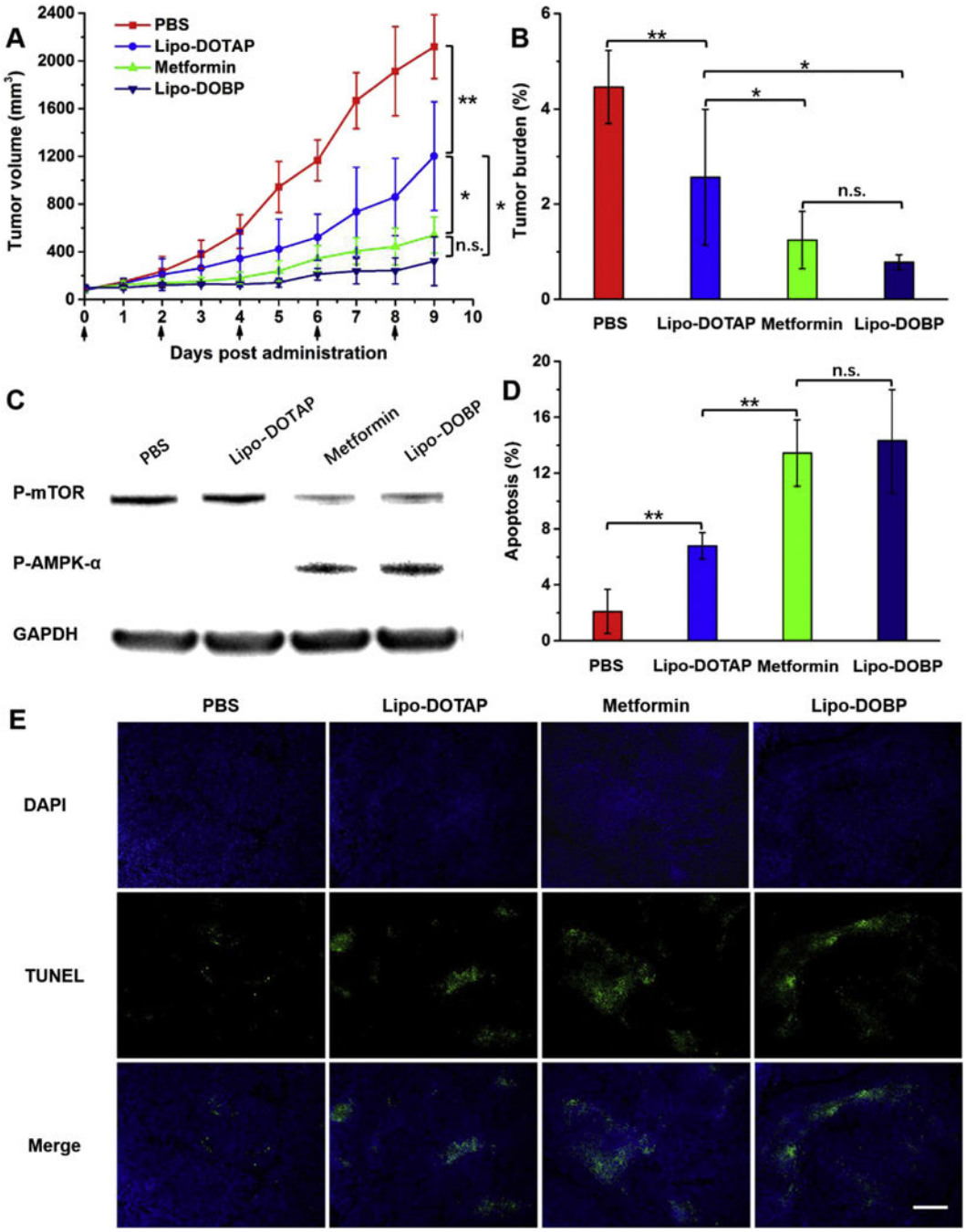

Fig. 5.

In vivo antitumor activity of blank liposomes (n = 5). (A) Tumor growth curves. (B) Tumor burden, the weight of tumors was divided by the average body weight of mice. (C) Western blot results. (D) TUNEL assay quantitative results of tumor sections treating with different formulations by Image J software. (E) TUNEL assay pictures of tumor sections treating with different formulations. The data are presented as means ± SD, $*P < 0.05$ and $**p < 0.01$. Scale bar represents 500 μm.

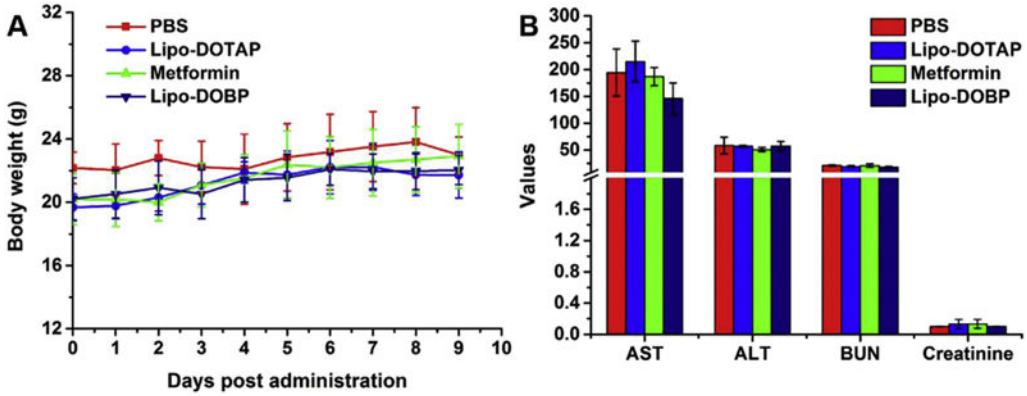

Fig. 6.

(A) Body weight changes and (B) hepatic and renal function indicators of mice bearing H460 tumor xenografts after treatment with blank liposomes (n = 5). No significant difference.

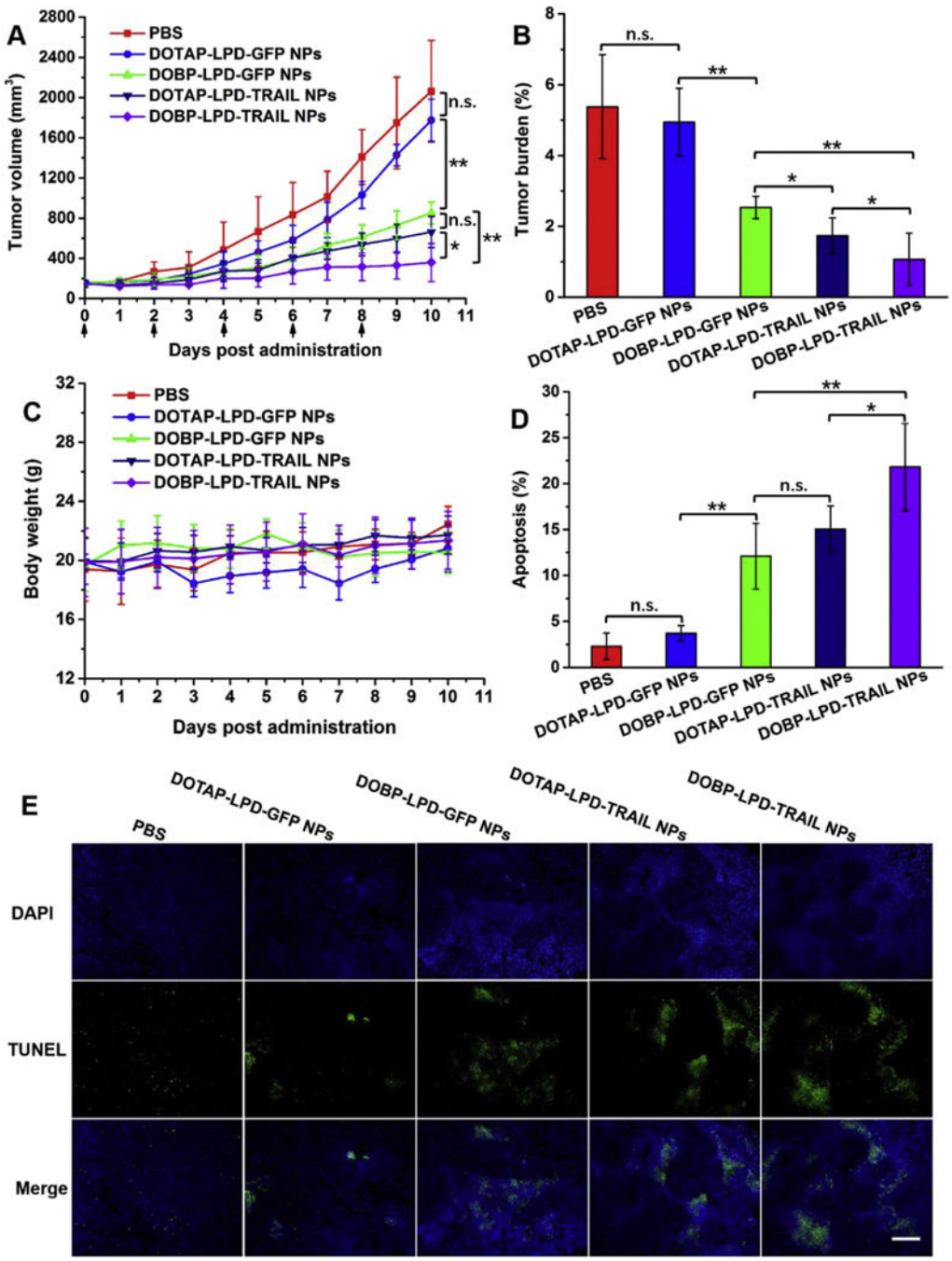

Fig. 7.

In vivo antitumor activity of LPD NPs (n = 5). (A) Tumor growth curves. (B) Tumor burden, the weight of tumors was divided by the average body weight of mice. (C) Body weight changes. (D) TUNEL assay quantitative results of tumor sections treating with different formulations by Image J software. (E) TUNEL assay pictures of tumor sections treating with different formulations. The data are presented as means ± SD, $*P < 0.05$ and $**p < 0.01$. Scale bar represents 500 μm.

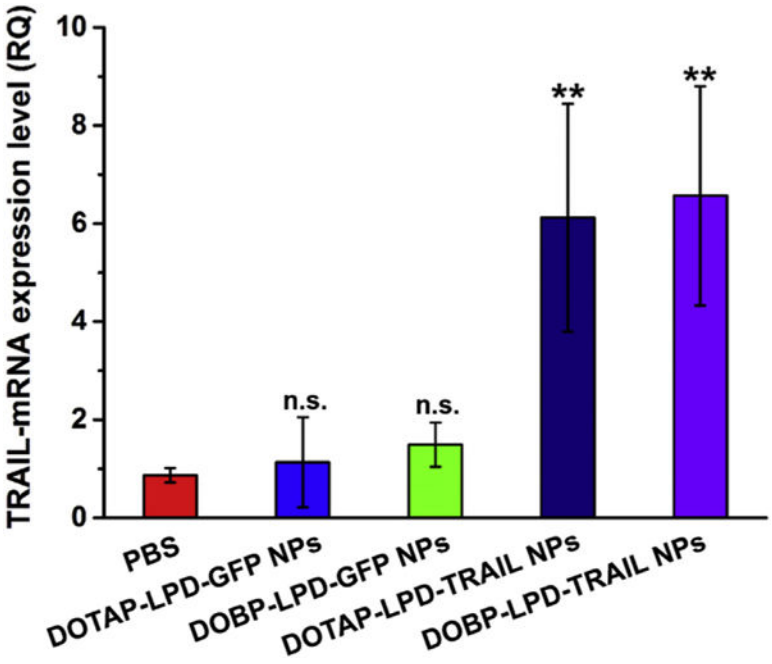

Fig. 8.

In vivo transfection of TRAIL plasmids. Difference from PBS group, $^{**}P < 0.01$.